ChemComm

Accepted Manuscript

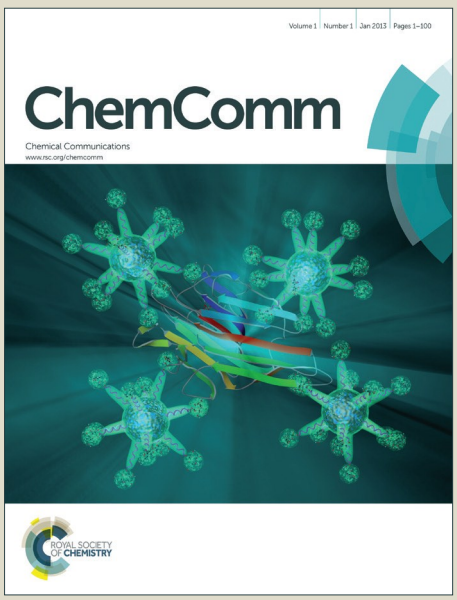

ROYAL SOCIETY OF CHEMISTRY

www.rsc.org/chemcomm

Journal Name

RSCPublishing

View Article Online
DOI: 10.1039/C5CC02383A

COMMUNICATION

Selective Endocytic Trafficking in Live Cells with Fluorescent Naphthoxazoles and their Boron Complexes

Cite this: DOI: 10.1039/x0xx00000x

Received 00th January 2014,
Accepted 00th January 2014

DOI: 10.1039/x0xx00000x

www.rsc.org/

Gleiston G. Dias,[a] Bernardo L. Rodrigues,[a] Jarbas M. Resende,[a] Hállen D. R. Calado,[a] Carlos A. de Simone,[b] Valter H. C. Silva,[c] Brenno A. D. Neto,[d] Marilia O. F. Goulart,[e] Fabricia R. Ferreira,[e] Assuero S. Meira,[f] Claudia Pessoa,[f,g] José R. Correa*[d] and Eufrânio N. da Silva Júnior*[a]

Fluorescent naphthoxazoles and their boron derivatives have been synthesized and applied as superior and selective probes for endocytic pathway tracking in live cancer cells. The best fluorophores were compared with the commercially available acridine orange (co-staining experiments), showing far better selectivity.

Endocytosis, as the key regulator process for molecular internalization in eukaryotic cells, has a fundamental role in cell homeostasis.[1] Signal transduction, neurotransmission, intercellular communication and immune response are known to be readily affected by endocytic pathway dysfunction.[2] The complexity of the cellular environment renders the understanding of endocytosis as an outstanding challenge. Cellular homeostasis, for instance, depends on the proper communication of the cellular organelles and all other components associated with correct signals throughout the highly complex machinery. Deregulation in any of these signalizing pathways could be the answer which triggers a specific pathological process. All homeostasis unbalances may also be associated with endocytosis dysfunctions. Fluorescence techniques, in this sense, rose up, shedding light onto many doubts over cellular endocytic mechanisms and pathways.[3] Despite the great advance of using fluorescent bioprobes,[4-7] many unanswered questions and challenges still remain to be tackled. For some, the capacity of a bioprobe to transpose the cell membrane is one of the most desirable features.[8] Very recently, some have shown the great potential of fluorogenic probes for studying dynamic cellular uptake in live cells.[9]

With the knowledge that many quinonoid derivatives sustaining the basic carbon scaffold are capable of transposing the cell-membrane and can present luminescence, as we[10-12] and others[13-15] have already demonstrated, we envisaged the synthesis of fluorescent bioprobes from an affordable naturally occurring naphthoquinone. In this sense, we aimed to use the cell membrane permeability feature of such compounds to synthesize fluorescent derivatives for dynamics and uptake in live cells using the endocytic pathway. Herein, we disclose the rational design, synthesis, characterization, single crystal X-ray, photophysics, DFT calculations, bioimaging, cellular uptake and dynamics in living cells (cancer cells) of new fluorescent derivatives which have allowed for selectively visualizing the whole endocytic pathway.

The structures of the synthesized fluorescent compounds are visualized in Figure 1 and the synthetic details are found in the supplementary material (Scheme S1).

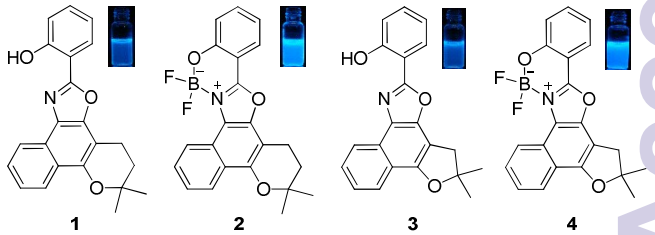

Figure 1. Structures of the fluorescent compounds evaluated in this work. Inset: fluorescence images under UV light (365 nm) in CH_2Cl_2 (50 μM).

All compounds afforded single crystals suitable for X-ray characterization (Figure 2 and Tables S5 and S6) with different packing depending on the size of the side ring.

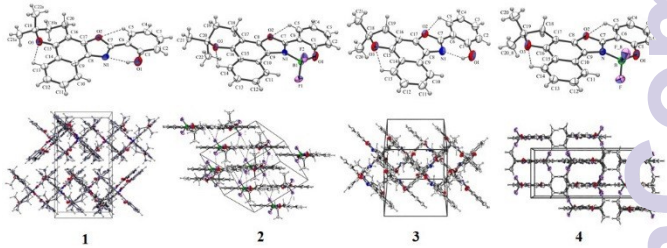

Figure 2. Molecular structure of **1**-**4** (top) and packing (bottom) depicted from single crystal X-ray analysis.

Molecular structures of **1** and **2** are basically planar except for the side pyrane ring. Compound **4** is in turn perfectly planar with methyl groups and fluorine atoms out of the plane. Distinct crystal packing for all compounds are also noted when comparing the four structures (Figure 2).

The photophysical properties of these molecules were investigated and pointed to the stability of these compounds in the excited state, as shown in Table 1.

Table 1. UV-Vis and fluorescence emission data (in different solvents) for **1**, **2**, **3** and **4** (10 μM of concentration).

Compound	Solvent	λ_{max} (abs) (nm)	λ_{max} (em) (nm)	Stokes shift (nm)
	Hexane	348	396	48
	CH_3Ph	353	402	49
	CH_2Cl_2	351	407	56
1	EtOAc	350	403	53
	MeOH	348	470	122
	MeCN	348	412	64
	DMSO	353	414	61
	Hexane	348	421	73
	CH_3Ph	353	433	80
	CH_2Cl_2	371	445	74
2	EtOAc	350	477	127
	MeOH	348	469	121
	MeCN	348	461	113
	DMSO	352	412	60
	Hexane	354	398	44
	CH_3Ph	358	409	51
	CH_2Cl_2	357	414	57
3	EtOAc	355	408	53
	MeOH	354	410	56
	MeCN	354	416	62
	DMSO	359	419	60
	Hexane	373	427	54
	CH_3Ph	378	445	67
	CH_2Cl_2	377	442	65
4	EtOAc	355	411	56
	MeOH	355	412	57
	MeCN	355	422	67
	DMSO	359	417	58

The quantum yields measured in triplicate with the respective standard deviations are 0.80 ± 0.07, 0.58 ± 0.05, 0.61 ± 0.05 and 0.42 ± 0.03.

In a general way, the boron complexes showed larger Stokes shift values, most likely due to the higher planarity and more efficient π-conjugation. Bathochromic displacements are observed when structures **1** and **3** were compared with their correspondent boron complexes, showing that the planarity introduced with the formation of the complex favors more electronic conjugation in the structure. Beyond the red shift, **3** and **4** displayed a shoulder at 356 and 360 nm, respectively, indicating an slight effect over its conformation as a consequence of the solvatochromic effect. The Stokes shifts for the BODIPY-like compound **2** are larger than those observed for the other structures (Table 1).

Considering the solvent effect is important for investigating this sort of derivatives, especially in the presence of polar solvents, therefore some theoretical calculations were performed aiming to shed some light on their behaviour in the ground and excited state. In this sense, DMSO was used (implicit treatment) as the medium for the calculations at PBE1PBE/6-311+G(2d,p)//CAM-B3LYP/6-31+g(d) level of theory. HOMO, LUMO (basically of π-type) and electron density difference were also calculated and are in accordance with the good stability observed in the excited state for compounds **1-4** (Figure S3).

View Article Online
DOI: 10.1039/C5CC02383A

Electrochemical (cyclic voltammetry, CV) analyses were also performed (Figures S45-S46). All the analysed compounds were reduced in two reduction waves (Figure S45 and Table S9). The first electron uptake was associated with a relatively stable radical anion whereas the second one is, presumably, a dihydro derivative, in accordance with similar compounds.[16] Differences in current were noticed comparing the boron-free and boron containing derivatives. As shown in Figures S45-46, comparison of the synthesized compounds allowed us to suggest that complexation with boron slightly facilitates the reduction process (Table S9), with E_{pc} values less negative than those for the boron-free compounds.

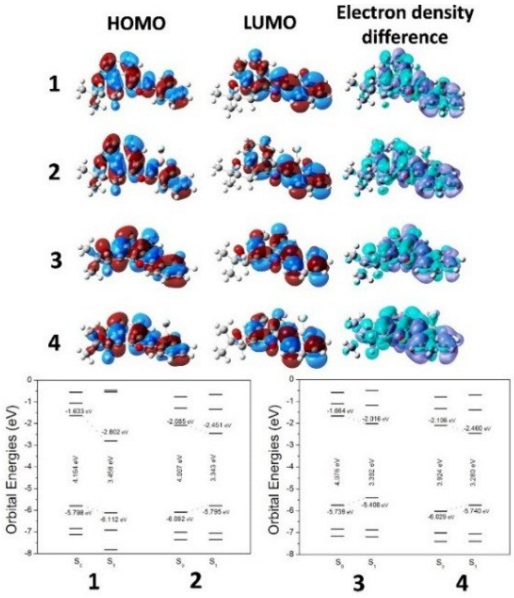

Figure 3. Optimized geometries, HOMO and LUMO plots, and electron density difference map. Diagram energy levels calculated with DMSO as the solvent. Calculations at PBE1PBE/6-311+G(2d,p)//CAM-B3LYP/6-31+g(d) level of theory. Structures calculated with implicit DMSO as the solvent showed similar orbitals localizations.

Finally, live cell-imaging experiments (PC3 cell lineages - human prostate cancer cells) were conducted to evaluate the potential of the fluorescent compounds as bioprobes. Dye **1** showed no fluorescent signal when incubated with live cells (Figure S41) whereas compounds **2-4** displayed a bright blue emission signal. These three compounds proved to be capable of staining the canonical endocytic pathway, meaning they are capable of selectively staining early endosome, late endosome and lysosome (Figures 4-6) during the cellular uptake process.

Panels (A) and (C) in Figures 4-5 show all membranous compartments strongly stained; there are no fluorescent signals inside of the nucleus. Acridine orange (AO) is widely used in order to stain endocytic pathways, however, AO also stains nucleic acids as can be observed in Figures 4-6. Under the same experimental conditions, **2-4** did not stain nucleic acids and the cell nuclei are visualized as black voids. Compounds **2**, **3** and **4** could be found at different localizations inside the cytoplasm and therefore are found associated with different membranous compartments. Vesicles found at the cell periphery close to the plasmatic membrane is correlated with early endosomes (Figure 4 and 5). Vesicles found between the plasmatic membrane and

the nucleus are correlated with late endosomes (Figures 5), whereas vesicles found near to the nucleus are correlated with lysosomes (Figure 6). The overlay images between the tested compounds and acridine orange (panel (C) in the cited Figures) provided the evidence that these compounds are staining the membranous compartments belonging to the endocytic pathway, but in this case selectively. AO is widely used to stain acidic organelles in studies regarding the endocytic and autophagic pathways applied to eukaryotic cells, however, as demonstrated, with high affinity to nucleic acid components, which produce a non-specific pattern in the cells nuclei. **2-4** were able to stain specifically the membranous compartments belonging to the endocytic pathway without nucleus cross staining.

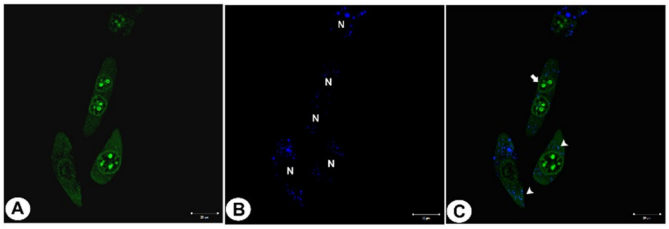

Figure 4. Live PC3 cancer cells stained with **2** (blue emission). (A) Positive control with cells stained with acridine orange (green emission). (B) **2** as the bioprobe and (C) Overlay of (A) and (B). **2** was found accumulated inside of spherical membranous organelles associated with endosomes (white arrow heads). White arrows show the nucleus stained with acridine orange (non-specific staining). N = cell nucleus. Reference scale bar 20 µm.

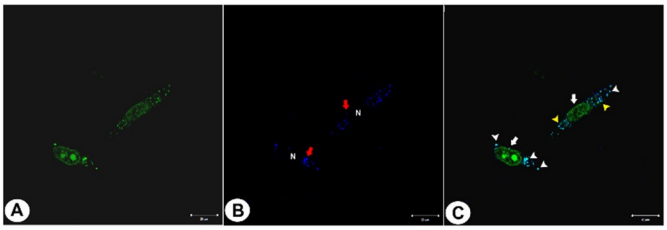

Figure 5. Live PC3 cancer cells stained with **3** (blue emission). (A) Positive control with cells stained with acridine orange (green emission). (B) **3** as the bioprobe and (C) Overlay of (A) and (B). **3** was found accumulated inside of spherical membranous organelle correlated with early endosomes (white arrow heads), late endosomes (yellow arrow heads) and lysosomes (red arrows). White arrows show the nucleus stained with acridine orange (non-specific staining). N = cell nucleus. Reference scale bar 20 µm.

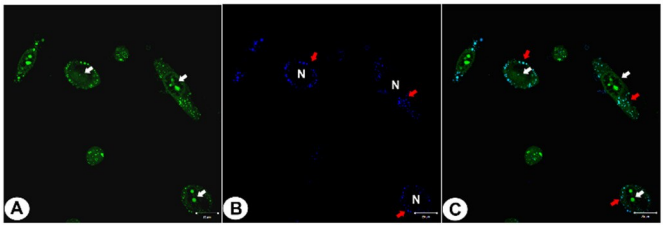

Figure 6. Live PC3 cancer cells stained with **4** (blue emission). (A) Positive control with cells stained with acridine orange (green emission). (B) **4** as the bioprobe and (C) Overlay of (A) and (B). **4** was localized inside of spherical membranous organelles belong to the endocytic pathway. Red arrows show the staining membranous compartment correlated with lysosomes. White arrows show the nucleus stained with acridine orange (non-specific staining). N = cell nucleus. Reference scale bar 20 µm.

The possibility of caveolae-mediated endocytosis was also evaluated to confirm the selective endocytic trafficking. Cells through caveolae-mediated endocytosis may also internalize the tested compounds irrespective of any affinity with the caveolar structure. Caveolar vesicles formation is a stable structure due to the lipids composition in these regions.[17,18] This feature keeps the vesicles open by a time period greater than that observed in membrane regions associated with clathrin-mediated vesicle formation.[17,19] Most likely the tested compounds accumulate in the open vesicles during their formation. As a consequence they are found trapped inside the vesicles during their bud off from the cells membrane therefore targeting the endoplasmic reticulum and matching with our finds related to vesicles staining near to the nuclei. To be sure about this hypothesis, an assay using the commercially available anti-caveolin-1 antibody (red emitter), which is the universal marker specific for caveolae vesicle formation, has been performed (Figures 7-9).

View Article Online
DOI: 10.1039/C5CC02383A

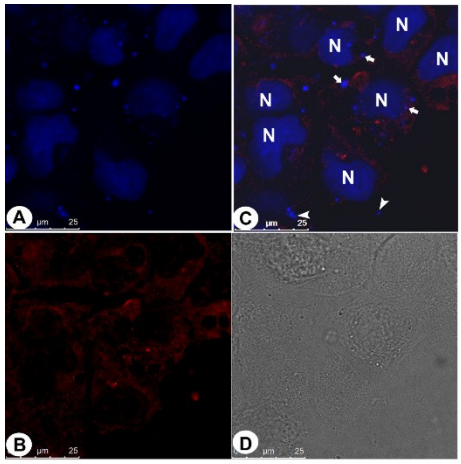

Figure 7. Live PC3 cancer cells stained with **2** and immunodetection of caveolin-1 (universal caveolar marker). (A) Shows the cell nucleus stained with commercially available DAPI (blue), and the cytoplasmic endocytic vesicles stained by each **2** (also in blue). (B) Shows the fluorescence distribution related to caveolin-1 immunodetection (red). (C) Shows the overlay of the two fluorescent signals (blue and red). Arrows show vesicles belong to canonical endocytic pathways (absence of caveolin-1 detection) and arrowheads show the vesicles belonging to caveolae-mediated endocytosis (vesicle with double staining - blue and red). (D) Shows the cells normal morphological aspects. Reference scale bar 25 µm.

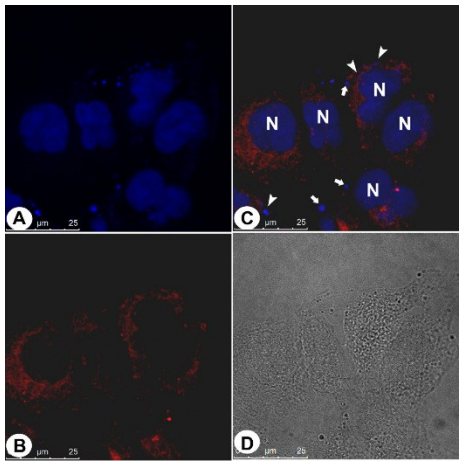

Figure 8. Live PC3 cancer cells stained with **3** and immunodetection of caveolin-1. (A) Shows the cell nucleus stained with DAPI (blue), and the cytoplasmic endocytic vesicles stained by each **3** (also in blue). (B) Shows the fluorescence distribution related to caveolin-1 immunodetection (red). (C) Shows the overlay of the two fluorescent signals (blue and red). Arrows show vesicles belong to canonical endocytic pathways (absence of caveolin-1 detection) and arrowheads show the vesicles belonging to caveolae-mediated endocytosis (vesicle with double staining

- blue and red). (D) Shows the cells normal morphological aspects. Reference scale bar 25 µm.

Figure 7 shows few vesicles stained near to cytoplasmic membrane correlated with caveolar vesicle bud off and near to the nucleus of the cell. This feature indicates the vesicles target endoplasmic reticulum which is the main docking point for caveolar vesicles. In other words, the caveolar entering is one possibility as well as the canonical endocytic pathway. The same behaviour could be noted for all tested compounds indicating the new bioprobes are capable of probing selectively the endocytic trafficking in live cells irrespective of the preferred internalization path. Similar results from that in Figure 7 have been observed in Figures 8 and 9.

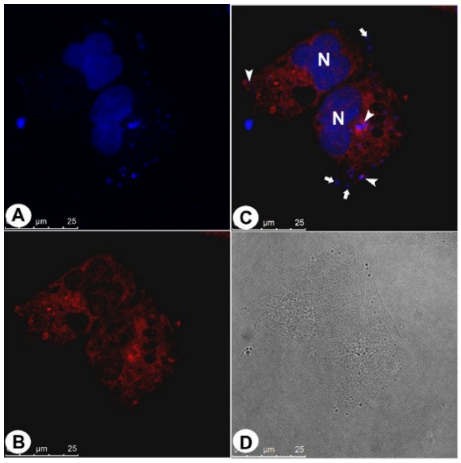

Figure 9. Live PC3 cancer cells stained with **4** and immunodetection of caveolin-1. (A) Shows the cell nucleus stained with DAPI (blue), and the cytoplasmic endocytic vesicles stained by each **4** (also in blue). (B) Shows the fluorescence distribution related to caveolin-1 immunodetection (red). (C) Shows the overlay of the two fluorescent signals (blue and red). Arrows show vesicles belong to canonical endocytic pathways (absence of caveolin-1 detection) and arrowheads show the vesicles belonging to caveolae-mediated endocytosis (vesicle with double staining - blue and red). (D) Shows the cells normal morphological aspects. Reference scale bar 25 µm.

In summary, four new fluorescent derivatives have been synthesized, characterized and successfully used as live cell-imaging probes, capable of selectively staining the endocytic pathway. The compounds also showed no cytotoxicity when evaluated by MTT assay. Compounds **2-4** were able to permeate intact live cells, thus being trapped inside of acidic compartments, turning them into suitable molecules for investigating the lysosome biogenesis, host pathogens interaction and autophagic processes, as will be disclosed in due course. The selective endocytic trafficking in live cells and its dynamics have been probed using the synthesized compounds, which in turn, were capable of selectively reveal the internalization endocytic process in live cell through both the caveolar vesicles or the canonical pathway. The new designed bioprobes showed by far better results than the commercially available AO. The authors would like to thank CAPES, CNPq, FAPDF, DPP-UnB, FINATEC and FAPEMIG.

Notes and references

[a] Institute of Exact Sciences, Department of Chemistry, Federal University of Minas Gerais, 31270-901, Belo Horizonte, MG, Brazil. E-mail: eufranio@ufmg.br

[b] Institute of Physics, Department of Physics and Informatics, University of São Paulo, 13560-160, São Carlos, SP, Brazil.

[c] University Unit of Exact Sciences and Technology, State University from Goiás, 75024-010, Anápolis, GO, Brazil.

[d] Laboratory of Medicinal & Technological Chemistry, Institute of Chemistry, University of Brasilia, 70904970, P.O.Box 4478, Brasilia, DF, Brazil. E-mail: correa@unb.br

[e] Institute of Chemistry and Biotechnology, Federal University of Alagoas, 57072-970, Maceió, AL, Brazil.

[f] Department of Physiology and Pharmacology, Federal University of Ceará, 60430-270, Fortaleza, CE, Brazil.

[g] Fiocruz-CE, 60180-900, Fortaleza, CE, Brazil.

View Article Online
DOI: 10.1039/C5CC02383A

Electronic Supplementary Information (ESI) available: [details of any supplementary information available should be included here]. See DOI: 10.1039/c000000x/

1. M. N. Levine, T. T. Hoang and R. T. Raines, *Chem. Biol.*, 2013, **2**, 614-618.
2. S. D. Conner and S. L. Schmid, *Nature*, 2003, **422**, 37-44.
3. A. A. Marti, S. Jockusch, N. Stevens, J. Ju and N. J. Turro, *Acc. Chem. Res.*, 2007, **40**, 402-409.
4. L. D. Lavis and R. T. Raines, *ACS Chem. Biol.*, 2014, **9**, 855-866.
5. L. D. Lavis and R. T. Raines, *ACS Chem. Biol.*, 2008, **3**, 142-155.
6. N. Johnsson and K. Johnsson, *ACS Chem. Biol.*, 2007, **2**, 31-38.
7. (*a*) B. A. D. Neto, J. R. Correa and R. G. Silva, *RSC Adv.*, 2013, **3**, 5297-5301. (*b*) B. A. D. Neto, J. R. Corrêa, P. H. P. R. Carvalho, D. C. B. L. Santos, B. C. Guido, C. C. Gatto, H. C. B. de Oliveira, M. Fasciotti, M. N. Eberlin and E. N. da Silva Júnior, *J. Braz. Chem. Soc.*, 2012, **23**, 777-781. (*c*) P. H. P. R. Carvalho, J. R. Correa, B. C. Guido, C. C. Gatto, H. C. B. De Oliveira, T. A. Soares and B. A. D. Neto, *Chem.-Eur. J.*, 2014, **20**, 15360-15374. (d) C. D'Angelis do E. S. Barbosa, J. R. Corrêa, G. A. Medeiros, G. Barreto, K. G. Magalhães, A. L. de Oliveira, J. Spencer, M. O. Rodrigues and B. A. D. Neto, *Chem. -Eur. J.*, 2015, **21**, 5055-5060.
8. A. Nadler and C. Schultz, *Angew. Chem., Int. Ed.*, 2013, **52**, 2408-2411.
9. A. A. R. Mota, P. H. P. R. Carvalho, B. C. Guido, H. C. B. de Oliveira, T. A. Soares, J. R. Correa and B. A. D. Neto, *Chem. Sci.*, 2014, **5**, 3995-4003.
10. E. H. G. da Cruz, P. H. P. R. Carvalho, J. R. Correa, D. A. C. Silva, E. B. T. Diogo, J. D. de Souza Filho, B. C. Cavalcanti, C. Pessoa, H. C. B. de Oliveira, B. C. Guido, D. A. da Silva Filho, B. A. D. Neto and E. N. da Silva Júnior, *New J. Chem.*, 2014, **38**, 2569-2580.
11. S. N. Sunassee, C. G. L. Veale, N. Shunmoogam-Gounden, O. Osoniyi, D. T. Hendricks, M. R. Caira, J.-A. de la Mare, A. L. Edkins, A. A. Pinto, E. N. da Silva Júnior and M. T. Davies-Coleman, *Eur. J. Med. Chem.*, 2013, **62**, 98-110.
12. E. N. da Silva Júnior, C. F. de Deus, B. C. Cavalcanti, C. Pessoa, L. V. Costa-Lotufo, R. C. Montenegro, M. O. de Moraes, M. C. F. R. Pinto, C. A. de Simone, V. F. Ferreira, M. O. F. Goulart, C. K. Z. Andrade and A. A. V. Pinto, *J. Med. Chem.*, 2010, **53**, 504-508.
13. (a) R. Araya-Maturana, W. Cardona, B. K. Cassels, T. Delgado-Castro, J. Ferreira, D. Miranda, M. Pavani, H. Pessoa-Mahana, J. Soto-Delgado and B. Weiss-Lopez, *Bioorg. Med. Chem.*, 2006, **14**, 4664-4669. (b) C. E. M. Carvalho, A. S. Silva, I. M. Brinn, A. V. Pinto, M. C. F. R. Pinto, S. Lin, T. A. Moore, D. Gust and M. Maeder, *Phys. Chem. Chem. Phys.*, 2002, **4**, 3383-3389. (c) C. E. M. Carvalho, I. M. Brinna, A. V. Pinto, M. C. F. R. Pinto, *J. Photoch. Photobio. A*, 1999, **123**, 61-65.
14. V. P. Torchilin, *Adv. Drug Deliv. Rev.*, 2005, **57**, 95-109.
15. E. M. Perchellet, B. J. Sperfslage, G. Qabaja, G. A. Jones and J. P. Perchellet, *Anti-Cancer Drugs*, 2001, **12**, 401-417.
16. Henning L., Ole H. Organic Electrochemistry. 4th Edition, Marcel Dekker, Inc, New York, 2001.
17. L. Pelkmans and A. Helenius, *Traffic*, 2002, **3**, 311-320.
18. A. Zloza, D. W. Kim, J. Broucek, J. M. Schenkel and H. L. Kaufman, *J. Interferon Cytokine Res.*, 2014, **34**, 915-919.
19. G. Sowa, *Front. Physiol.*, 2012, **2**, 120.